Unravelling local atomic order of the anionic sublattice in $M(Al_{1-x}Ga_x)_4$ with M = Sr and Ba by NMR spectroscopy and quantum mechanical modelling

Oliver Pecher,[a,b,c], Bernhard Mausolf,[a] Volker Peters,[a] Kevin Lamberts,[a] Alexander Korthaus,[a] and Frank Haarmann*[a,b]

Dedication ((optional))

Abstract: The quasi-binary section of the intermetallic phases MAl_4 and MGa_4 with M = Sr, Ba have been characterised by means of X-ray diffraction (XRD) and differential thermal analysis. The binary phases show complete miscibility forming solid solutions $M(Al_{1-x}Ga_x)_4$ with M = Sr, Ba. They crystallise in the $BaAl_4$ structure type with four and five bonded Al and/or Ga atoms, denoted as Al(4b), Al(5b), Ga(4b), and Ga(5b), respectively, forming a polyanionic Al—Ga sublattice. Solid-state ^{27}Al NMR and quantum mechanical (QM) calculations were applied to study the bonding of Al and the influence of Al/Ga substitution, especially in the regimes of low substitutions degrees. $M(Al_{1-x}Ga_x)_4$ with M = Sr, Ba and $0.925 \leq x \leq 0.975$ can be described as a matrix of the binary majority compound in which a low amount of the Ga atoms is substituted by Al. In good agreement with QM calculations, ^{27}Al NMR and single-crystal XRD proof a preferred occupancy of Al(4b) for these substitution regimes. Furthermore, two different local Al environments are found: isolated Al(4b1) atoms as well as Al(4b2) due to the formation of Al(4b)—Al(4b) pairs besides the isolated Al(4b) atoms within the polyanionic sublattice. QM calculations of the electric field gradient (EFG) using superlattice structures within periodic boundary conditions are in good agreement with the NMR results and discussed in detail.

Introduction

Intermetallic phases (IPs) are a fascinating class of materials with numerous applications such as superconductors[1–3], spintronics[4,5], thermoelectrics[6–8], and catalysis materials[9]. Further insights into the structure-bonding-property relationships of IPs is still a sought-after issue nonetheless to improve technical applications and to make existing industrial usage even more efficient.[10–16] Especially materials showing atomic disorder and low amounts of dopants are an interesting field for both research[13–19] and applications, e.g. semiconductors,[20–22] steel,[23] and battery materials.[24]

In particular, the $BaAl_4$ structure type is highly important for IPs.[25] It is furthermore realised in various three dimensional (3D) ordered variants such as $ThCr_2Si_2$ or $TlCu_2Se_2$.[26,27] $ThCr_2Si_2$ and $TlCu_2Se_2$ possess a separation of the different atom types on the two crystallographic sites of the anionic sublattice; a significantly different c/a ratio within the $BaAl_4$ type unit cell results. In contrast, an atomic ordering of mixed occupied sites is found for $CaBa_2Ge_2$. In addition, larger unit cells with varying colouring schemes of the two crystallographic sites of the anionic sublattice are reported as super lattice structures of the $BaAl_4$ type.[28,29]

The combined application of X-ray diffraction (XRD), solid-state nuclear magnetic resonance (NMR) spectroscopy and quantum mechanical (QM) calculations was recently shown to be well suited to study the chemical bonding and local atomic environments in ordered and disordered IPs.[18,30] The XRD—NMR—QM approach was thereby applied to the binary IPs MGa_2 with M = Ca, Sr, and Ba[31] as well as MGa_4 with M = Na, Ca, Sr, and Ba[32] to gain insights into the chemical bonding of the Ga atoms. An analysis of the electric field gradient (EFG) turned out to be a sensitive local measure for different chemical environments of the Ga atoms. Furthermore, we recently showed that the approach is suited to study varying Ga bonding situations due to cation substitution in the solid solution $Sr_{1-x}Ba_xGa_2$.[33] Similar attempts have been reported for complex types of substitution of the alkaline earth metals in $Sr_{1-x}Ga_{2+3x}$ and $Ca_{1-x}Ga_{2+3x}$ as well as vacancies influencing the Cu bonding in $Cu_{1-x}Al_2$.[17,34–38]

In this contribution we report on the next step by focussing on the difference of Al representing a typical main group metal vs. Ga being a non-typical main group metal. The influence of substitution on the chemical bonding within the anionic sublattice in $M(Al_{1-x}Ga_x)_4$ with M = Sr, Ba is addressed in the following. The binaries crystallise in the $BaAl_4$ type of structure in space group $I4/mmm$ (Figure 1).[17,32]

[a] Dr. O. Pecher, Dipl.-Chem. B. Mausolf, V. Peters (M.Sc), Dr. K. Lamberts, Dipl.-Chem. A. Korthaus, Dr. F. Haarmann
RWTH Aachen University, Institut für Anorganische Chemie (IAC)
Landoltweg 1, 52074 Aachen (Germany)
E-mail: frank.haarmann@ac.rwth-aachen.de

[b] Dr. O. Pecher, Dr. F. Haarmann
Max-Planck-Institut für Chemische Physik fester Stoffe
Nöthnitzer Straße 40, 01187 Dresden (Germany)

[c] Dr. O. Pecher
Present address: University of Cambridge, Department of Chemistry
Lensfield Road CB2 1EW, Cambridge (UK)

Supporting information for this article is currently given at the end of the document.

d / Å	Al	Ga
Sr	2.665	2.616
Ba	2.713	2.676

d / Å	Al	Ga
Sr	2.689	2.570
Ba	2.707	2.592

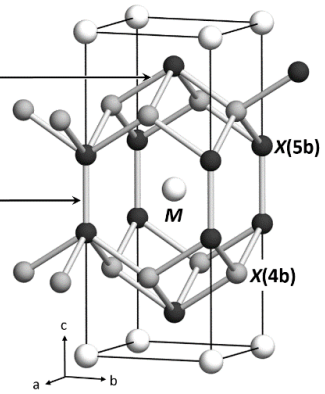

Figure 1. Crystal structures of MX_4 with *M* = Sr, Ba and *X* = Al or Ga in the $BaAl_4$ type of structure in space group *I*4/*mmm*. Four- and five-bonded Al or Ga atoms are indicated by *X*(4b) and *X*(5b). Black lines represent the unit cell and thick grey lines Ga—Ga and Al—Ga contacts, respectively. Atomic distances (*d* / Å) of the binary samples are given in the tables on the left.[12,19,20]

Four- and five-bonded Al(4b)/Ga(4b) and Al(5b)/Ga(5b) atoms, respectively, are found to build a three-dimensional polyanionic sublattice. In this context, the formulation as (*n*b) is not meant in the sense of two-electrons-two-centre bonds but describe interatomic distances that are smaller than the average Al—Al distance in Al (2.86 Å)[39] and Ga—Ga distance in α-Ga (2.70 Å)[40], respectively.[15,17,31,32]

As for cationic disorder in $Sr_{1-x}Ba_xGa_2$ a model of isolated substitution centres (ISC)[33] in the vicinity of low degrees of substitution was carved out. We extended this approach within the XRD—NMR—QM methodology to study $M(Al_{1-x}Ga_x)_4$ with *M* = Sr, Ba. An application of the ISC model on atomic disorder in the polyanionic sublattice of $M(Al_{1-x}Ga_x)_4$ with *M* = Sr, Ba is likely to increase the experimental resolution for NMR experiments, which is crucial to derive NMR coupling parameters throughout line shape analysis. In cases of too high amounts of atomic disorder in IPs this can be challenging up to impossible since characteristic NMR signal features are smeared out and important details of the line shape information get lost.[33]

Since NMR is a non-phase sensitive method, we performed a careful pre-characterisation of the materials under investigation using powder and single crystal XRD as well as differential thermal analysis (DTA) measurements for selected samples. Based on these results the lattice parameters, crystal structure and miscibility of $M(Al_{1-x}Ga_x)_4$ with *M* = Sr, Ba is reviewed. Afterwards, the local atomic order and NMR spectroscopy combined with the results from QM calculations of the EFG are discussed.

Results and Discussion

Powder XRD and Lattice Parameters

The synthesis of $M(Al_{1-x}Ga_x)_4$ with *M* = Sr, Ba results in single-phase materials (Experimental Section). No crystalline impurities or neighbouring phases were detected.

The powder XRD patterns are indexed in space group *I*4/*mmm* and show significant shifts of the sample reflections with respect to the substitution degree. A minimum of lattice parameter *a* is found for *x* = 0.5 while the *c* parameter decreases linearly from the aluminide to the gallide (Figure 2, Figure S 1, Table S 1).

Comparing the metallic radii of Al and Ga with 143.2 and 141.1 pm[37], respectively, a decrease of 1.5% is found although Ga is located one period below Al in the periodic table of the elements. This decrease is also indicated by the different lengths of the crystallographic *a* axis but not by the *c* axis (Figure 2, Figure S 1). $M(Al_{1-x}Ga_x)_4$ with *M* = Sr, Ba shows the larger lattice parameter for *x* = 0 than *x* = 1. Interestingly, the *c* parameter decreases linearly from *x* = 0 to 1, while *a* minimum is found for the *a* parameter at *x* = 0.5 (Figure 2, Figure S 1).

These anisotropic changes of the lattice are also indicated by the *c*/*a* ratios for $M(Al_{1-x}Ga_x)_4$ with *M* = Sr with 2.511 (*x* = 0) vs. 2.416 (*x* = 1) and *M* = Ba with 2.477 (*x* = 0) and 2.357 (*x* =1), respectively. This corresponds to a decrease of -4 and -5 % for the Sr and Ba case (Figure 2, **Error! Reference source not found.**, **Error! Reference source not found.**). Hence, the *c*/*a* ratio seems to be a good indicator for the changing bond lengths in $M(Al_{1-x}Ga_x)_4$ with *M* = Sr, Ba (Figure 1). A substitution of Al by Ga results in a decrease of the 4b—4b distance of -1.9 and -1.4 % as well as of the 5b—5b bond length of -4.6 and -4.4 % for Sr and Ba, respectively. Hence, the change of the *a* lattice parameter is within the range of the changes of the atomic radii and the changes of the *c* parameter mirror approximately the decrease of the 5b—5b distances.

The minimum of the *a* lattice parameter for $M(Al_{1-x}Ga_x)_4$ with *M* = Sr, Ba for *x* = 0.5 indicates a preferred occupancy of the Al(4b) position since the 4b—4b interaction within the *ab* plane is described as a multi-centre-electron-deficient one with metallic character and the 5b bonding along the *c* axis as a covalent two-electron-two-centre bond, respectively.[17,41] Solid-state ^{27}Al NMR investigations have been performed to shed light into this assumption (Section Solid-State NMR Spectroscopy). In addition, a discussion of the lattice parameter trends interpreted by means of the Ga—Ga, Ga—Al, and Al—Al interactions and their "bonding analysis" referring to the fundamental work of Miller *et al.*[41] can be found in the Supporting Information (Figure S1b and text).

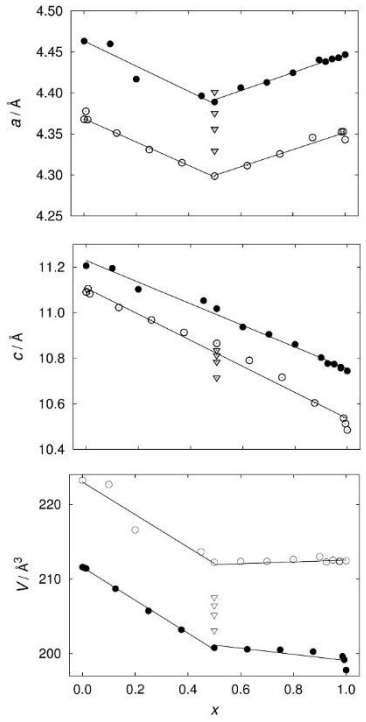

Figure 2. Lattice parameters *a* and *c* as well as unit cell volumes *V* of $Sr(Al_{1-x}Ga_x)_4$ in space group *I*4/*mmm*. Experimental and QM calculated data are depicted as full and open circles, respecitvely. Open triangles show various local ordering variants of Al(4b)/Al(5b) for $x = 0.5$. Error bars are within the symbols. A linear trend line corresponding to Vegard's rule is indicated by black lines. The data for $Ba(Al_{1-x}Ga_x)_4$ is shown in Figure S 1a.

DTA Measurements

DTA experiments of selected $M(Al_{1-x}Ga_x)_4$ with *M* = Sr, Ba samples confirm the congruent melting points 1040°C and 961°C for $Sr(Al_{1-x}Ga_x)_4$ with $x = 0.0$[42] and 1.0[31], respectively, as well as 1080°C and 1026°C for $Ba(Al_{1-x}Ga_x)_4$ with $x = 0.0$[43] and 1.0[31] (**Error! Reference source not found.**, Experimental Section). The maxima of the endothermic melting signal are continuously shifted from the low-melting component to the high-melting one with increasing amount of Al substitution. The DTA signals are broadened due to the substitutional disorder of the ternary compounds and the experimental resolution for $Ba(Al_{1-x}Ga_x)_4$ is worse, which indicates less crystalline materials in comparison with $Sr(Al_{1-x}Ga_x)_4$. For $Sr(Al_{1-x}Ga_x)_4$ with $x = 0.925$, 0.9, and 0.5 a less intense endothermic signal is detected just before the intense melting signal (**Error! Reference source not found.**). This DTA line shape indicates a small separation of *liquidus* and *solidus* line of the pseudo-binary system $SrAl_4$—$SrGa_4$.[33,44] Hence, $Sr(Al_{1-x}Ga_x)_4$ can be described as a solid solution of low-melting $SrGa_4$ and high-melting $SrAl_4$ with full miscibility. The $Ba(Al_{1-x}Ga_x)_4$ situation is similar but less pronounced in the DTA line shape due to a worse signal-to-noise ratio.[33,44]

Single Crystal XRD

The refinement of single crystal XRD data at 100(2) K for $Sr(Al_{1-x}Ga_x)_4$ with $x = 0.925$ verifies its composition to be $Sr(Al_{0.063(6)}Ga_{0.937(6)})_4$ (Table 1, Table 2, and Experimental Section). The refinements confirm a preferred occupancy of Al(4b) and exclude any significant occupancy of the Al(5b) position since negative site occupancy factors result.

Table 1. Single crystal X-ray data collection and parameters of the structure refinement for $Sr(Al_{1-x}Ga_x)_4$ with $x = 0.925$ at 100(2) K. The asterisk (*) refers to ambient temperature measurements.

Formula	$SrAl_{0.3}Ga_{3.7}$
T / K	100(2)
Formula weight / g mol^{-1}	353.68
Crystal size / mm	0.12 0.09 0.08
Crystal colour	Silver
Crystal system	Tetragonal
Space group	*I*4/*mmm* (No. 139)
a / Å (powder*/single-crystal)	4.4382(6) / 4.4189(9)
c / Å (powder*/single-crystal)	10.777(4) / 10.752(2)
V / Å^3 (powder*/single-crystal)	231.98(10) / 209.95(10)
Z	2
Diffractometer; detector	Bruker D8; Apex CCD, multilayer optics
λ / Å	0.71073 (MoK_α)
μ (MoK_α) mm^{-1}	35.903
ρ_{calc} / g cm^{-3}	5.5943
$2\theta_{max}$ / °	35.15
	$-5 \le h \le 6$, $-5 \le k \le 7$, $-15 \le l \le 17$
Measured reflections	1458
Independent reflections	185
R_{int}	0.0558
Obs. reflections $F_o > 4\sigma(F_o)$	167
Number of parameters	9
*R*1 ($F_o > 4\sigma(F_o)$) / *R*1 (all data)	0.0369 / 0.0409
*wR*2 ($F_o > 4\sigma(F_o)$) / *wR*2 (all)	0.0866 / 0.0882
Goodness of Fit (GooF)	1.021
Residual electron density (hole / peak) e / Å^{-3}	-3.005/2.617

Table 2a. Wyckoff positions, fractional atomic coordinates, and site occupancy factors (sof) of $Sr(Al_{1-x}Ga_x)_4$ with $x = 0.925$ at 100(2) K.

Atom	Site	*x*	*y*	*z*	*sof*
Sr	2*a*	½	½	½	1
Al(4b)	4*d*	½	0	¼	0.874(12)
Ga(4b)	4*d*	½	0	¼	0.126(12)
Ga(5b)	4*e*	½	-½	0.1167(1)	1

Table 2b. Displacement parameters of $Sr(Al_{1-x}Ga_x)_4$ with x = 0.925 at 100(2) K. All U_{ij} and U_{eq} values in Å^2. $U_{11} = U_{22}$; $U_{23} = U_{13} = U_{12} = 0$.

Atom	Site	U_{11}	U_{33}	U_{eq}
Sr	2*a*	0.0038(4)	0.0039(4)	0.0039(3)
Al/Ga(4b)	4*d*	0.0051(4)	0.0026(4)	0.0043(3)
Ga(5b)	4*e*	0.0042(4)	0.0025(4)	0.0036(3)

The displacement parameters for Al/Ga on (4b) were refined anisotropically but constrained to the same values for both atoms; Ga(5b) was also refined anisotropically. The resulting prolate shapes of both positions are aligned in *c*-direction and may be assigned to the general structure of the Ga-sublattice with a more rigid geometry in *a*-direction. The anisotropic refinement of Sr yielded an isotropic atom within standard deviations (Table 2). A further interpretation of this data does not seem to be suitable since despite the good reflection/refinement-parameter ratio of 189/9 (approx. 20.5) we observed a strong correlation of the U_{ij} values within the analysed *d* value range.

Furthermore, there is a significant correlation of U_{ij} with the site occupancy factors. The final refinement fulfils the quality requirements regarding the *R* and R_{int} values as well as the residual electron density (Table 1, Table 2, Experimental Section). Hence, a preferred occupancy of Al(4b) is proven by XRD.

Local Order of the Atoms

Based on the $BaAl_4$ structure type and the low substitution degree we estimate the distribution of Al(4b) in the unit cell for $M(Al_{1-x}Ga_x)_4$ with x = 0.925, 0.950, and 0.975. This substitution can be described as a matrix of MGa_4 with *M* = Sr, Ba with 2.5, 5.0, and 7.5 % Al substitution, which we will denote as Al@MGa_4 in the following. Regarding the formula sum the number of Al atoms per unit cell can be calculated by $(1-x)^{-1} \times ½ \times ¼$ where the $(1-x)^{-1}$ factor describes a respective "dilution" throughout a multiplication of the unit cell and this factor as the inverse value of the substitution degree with respect to the amount of Al; the factor ½ takes a preferred occupancy of the (4b) position into account and the multiplication with factor ¼ normalises this calculation on the number of formula units of the MGa_4 matrix. Considering a statistical distribution of the Al(4b), this estimation results in Al(4b) in every 5th, 2.5th, and 1.7th unit cell for 2.5, 5.0, and 7.5% Al@MGa_4. The statistical probability for Al@(4b) increases with increasing substitution degree; but even for 7.5 % Al@MGa_4 it is unlikely that more than one Al atom per unit cell occupies the (4b) position. Hence, the ISC model is formally fulfilled within the substitution regime discussed and under consideration of the crystal structure assumptions.

Solid-State NMR Spectroscopy

Frequency sweep NMR of the regular powder signals of MAl_4 with *M* = Sr, Ba show the central transition (CT) signals of Al(4b) and Al(5b) and their respective satellite transition (ST) signals spreading a frequency range of -750 to 1000 kHz (Figure 3, **Error! Reference source not found.** top).

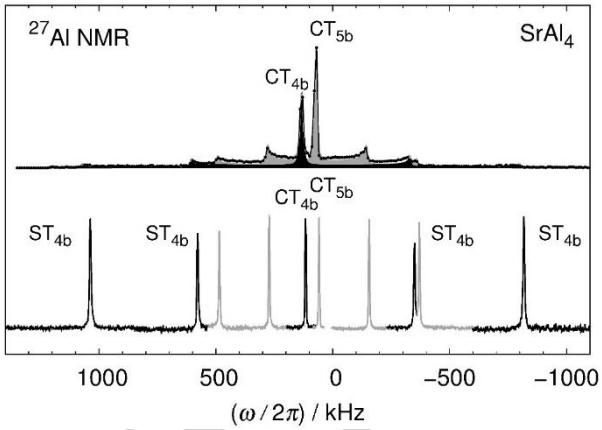

Figure 3. ^{27}Al NMR spectra of regular (top) and aligned (bottom) $SrAl_4$ powder. Central and satellite transitions are marked by CT and ST, respectively. Experimetal data is shown with solid lines and fits with black and grey shaded areas, respectively. NMR signal contributions of Al(4b) and Al(5b) are represented for the alligned powder in black and grey. The data for $BaAl_4$ is shown in **Error! Reference source not found.**.

The number of signals is in agreement with the crystal structure. An alignment of the crystallites in the magnetic field shows a significant enhancement of the experimental resolution, which results in sharp and easily distinguishable CT and ST signals for Al(4b) and Al(5b) (Figure 3, **Error! Reference source not found.** bottom). The signal detection of the aligned powders was performed with wideline NMR experiments applying different carrier frequencies due to the significantly different shift values (Figure 3, **Error! Reference source not found.** bottom, Experimental Section).

^{27}Al NMR investigations of $M(Al_{1-x}Ga_x)_4$ with *M* = Sr, Ba for x = 0.925, 0.950, and 0.975 show nearly complete disappearance of the CT_{5b} signal, which is more pronounced for *M* = Sr (Figure 4, **Error! Reference source not found.**). A measurement for the highest Al—Ga substitution degree, exclusively performed for $Sr(Al_{1-x}Ga_x)_4$ with x = 0.5, shows a CT_{5b} signal of very low intensity but still present (Figure 4). Furthermore, the ST signals are tremendously broadened, indicating a high degree of atomic disorder. A very low crystallinity of the investigated powder sample, already indicated by the thermoanalytical investigations, is likely to also cause this broadening in part (Section DTA Measurements).

Focussing on the ISC regimes, a preferred occupancy of the (4b) position for 2.5, 5.0, and 7.5 % Al@MGa_4 with *M* = Sr, Ba is indicated by an increase of the ST_{4b} intensities as well as frequency ranges (Figure 4, Figure S 4). Furthermore, the ST_{4b} signal line shape shows additional signal contributions, which are not caused by an isolated Al(4b) position (Figure 5, Figure S 5). Hence, on the local atomic scale of NMR, an additional Al environment is detected for 2.5, 5.0, and 7.5 % Al@MGa_4 with *M* = Sr, Ba. We assign this signal to a special local arrangement of Al(4b)—Al(4b) pairs besides isolated Al(4b) atoms within the polyanionic sublattice (Figure 5, left). We distinguish these different Al(4b) environments as Al(4b1) and Al(4b2), respectively (Figure 5).

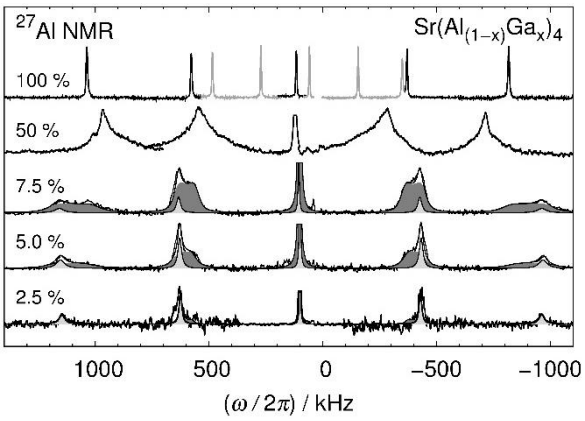

Figure 4. ^{27}Al NMR spectra of aligned powder samples of $Sr(Al_{1-x}Ga_x)_4$ with x = 0.0, 0.5, 0.925, 0.950, and 0.975 from top to bottom. NMR signal contributions of Al(4b1), Al(4b2) are shaded for Al content of 2.5, 5.0, and 7.5 % in light and dark grey, respectively. The data for $Ba(Al_{1-x}Ga_x)_4$ is shown in **Error! Reference source not found.**.

QM Calculations

The system $M(Al_{1-x}Ga_x)_4$ with M = Sr, Ba was studied by means of density functional theory (DFT) using VASP and WIEN2k program packages.[45,46] Lattice parameters, formation energies, crystal structure variations, local ordering of the atoms, and NMR parameters due to substitution in the anionic sublattice are in the focus of this investigation. Following the group-subgroup relations according to the Bärnighausen formalism[47] super lattice structures (SLS) were developed to describe the local atomic arrangements (Experimental Section). The symmetry relations and corresponding Wyckoff positions are summarised in Figure S 7.

The calculations were performed with the space group's symmetry restraints and without in space group $P1$ to double check on possible influences on the results throughout the symmetry restraints. Calculations for $P1$ structure models are much more expensive but offer detailed unaffected information about atomic shifts.

The electric field gradients (EFG) of the binary phases MX_4 with M = Sr, Ba and X = Al, Ga, In reflect the increasing polarizability of the group 13 elements by an increasing anisotropy of the charge distribution with the atomic number of the element (**Error! Reference source not found.**). The negative sign of V_{ZZ} obtained for all positions of the anionic sublattice indicates a prolate charge distribution that is aligned with V_{ZZ} along the c axis of the unit cell. The absolute values of the EFG's main component V_{ZZ} are larger for the 4b than for the 5b atoms, i.e. the electron distribution of the 4b atoms in the centre of a distorted tetrahedron is more elongated than for the 5b atoms in tetragonal pyramidal environment.

The respective V_{ZZ}(4b)/V_{ZZ}(5b) ratio decreases from 2.7 to 1.7 with increasing atomic number of the group 13 element. This is slightly less pronounced for the heavier alkaline earth metal indicating an interaction of the anionic sublattice with the cations.

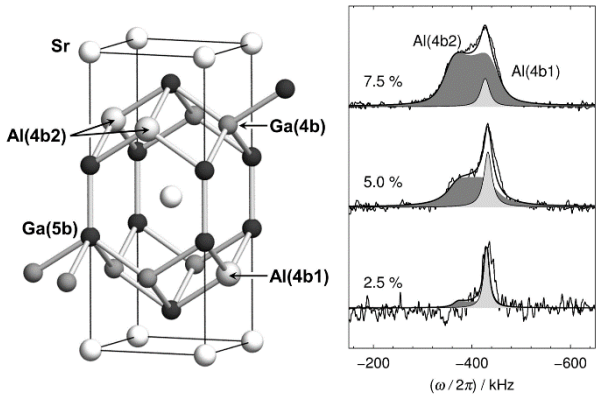

Figure 5. (Left) Crystal structure of $Sr(Al_{1-x}Ga_x)_4$ with x = 0.925, 0.950, and 0.975. Different local four-bonded Al(4b1) and Al(4b2) environments are indicated next to the four- and five-bonded Ga(4b) and Ga(5b) atoms of the anionic sublattice. (Right) Zoom of the inner ^{27}Al(4b) satellite transition NMR signals of $Sr(Al_{1-x}Ga_x)_4$ with x = 0.925, 0.950, and 0.975 corresponding to Al amounts of 2.5, 5.0, and 7.5 % from top to bottom. Experimental data is shown with solid black lines; contributions of Al(4b1) and Al(4b2) are given as light and dark grey shaded areas, respectively. The data for $Ba(Al_{1-x}Ga_x)_4$ is shown in **Error! Reference source not found.**.

V_{ZZ}(4b) of the Al atoms increases almost linearly with the number of next neighbour Ga atoms and is only subject to minor changes for geometric variations as shown by SLS calculations (**Error! Reference source not found.**). In comparison, V_{ZZ}(5b) is strongly influenced by the number of next neighbour Ga atoms. Furthermore, the individual local conformation possess a significant influence. The reason for that might be a higher sensitivity of the 5b position on chemical bonding and/or the much smaller absolute value of V_{ZZ}. Additionally, V_{ZZ}(5b) is quite sensitive on the positional z parameter of the atoms as shown by systematic variations of this parameter (**Error! Reference source not found.**).

V_{ZZ} of both Al sites is almost exclusively influenced in the first coordination sphere of the substitution centre (**Error! Reference source not found.**). Outside this range, a scattering around an average value close to the experimental ones of the binary parent phases is observed. In addition, the asymmetry parameter is influenced in higher coordination spheres but decreases to almost zero above 10 Å. A similar trend is found for the positional shifts of the atoms.

Optimisation of lattice parameter for various SLS results in a good agreement with the experimental values (Figure 2, **Error! Reference source not found.**). The systematic offset towards smaller values for all calculations is within the typical range, well known for the LDA over binding phenomenon.[48] Especially the experimentally observed minimum of the a parameter is well reproduced. A large influence of the local atomic order in the anionic sublattice is seen by a variation of Al(4b)/Al(5b) site occupation for x = 0.5 in $M(Al_{1-x}Ga_x)_4$ with M = Sr, Ba. Increasing and decreasing lattice parameter are obtained for a and c, respectively.

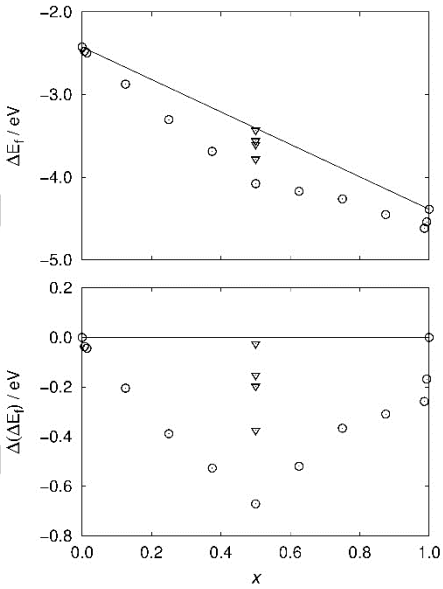

Additional evidence for a Al(4b) preferred site occupation is obtained by an estimation of the formation energies Δ_fE (Figure 6, **Error! Reference source not found.**). These were calculated as the difference between the total energy (E_{tot}) of the structure model (Md.) and the weighted total energies ($\sum E_{tot}$) calculated for the elements: $\Delta_f E = E_{tot}(Md.) - \sum E_{tot}(elem.)$.[48,49]

The resulting negative Δ_fE values indicate that all investigated structures are stable compared to the elements (Figure 6, **Error! Reference source not found.**). The differences of the formation energies $\Delta(\Delta_f E)[x(Ga)] = \Delta_f E[x(Ga)] + \Delta(\Delta_f E)[\text{binary phases}]\cdot[x(Ga)]$ of $M(Al_{1-x}Ga_x)_4$ (referenced to MGa_4 and MAl_4) with M = Sr, Ba show a concave trend visualising the relative stability. Hence, a preferred occupancy of the 4b position by Al is also indicated by energetic considerations. This stabilisation effect is even more pronounced for the Sr than the Ba phase (Figure 7).

Various 3×3×2 SLS models were applied to model local atomic coordinations at low substitution degrees and explore the origin of the experimentally observed Al(4b2) NMR. Model I (*Md. I*) describes two Al(4b) separated by a distance lager than 10 Å. The other SLS calculations focus on local arrangements within the $BaAl_4$ type unit cell surrounded by a MGa_4 matrix with M = Sr, Ba (Figure 7). Two neighbouring Al(4b) sites with shortest Al—Al distances of approx. 3.1 Å were used in *Md. II. Md. III* focuses on a formation of Al(4b)—Al(4b) pairs within the *ab* plane of the unit cell (d ≈ 4.4 Å) and *Md. IV* on such pairs along the c axis (d ≈ 5.4 Å). *Md. V* describes the remaining Al(4b)—Al(4b) pairs with a distance of approx. 6.2 Å within a $BaAl_4$ type unit cell. The overall variation of the energy is below 0.01 eV and is even smaller for $Ba(Al_{1-x}Ga_x)_4$. Thus, compared with the thermal energy available at ambient temperature none of these models is favourable with respect to energetic reasons (**Error! Reference source not found.**).

The changes of V_{ZZ}(4b) for models *Md. I* to *Md. V* are very small (± 3%). *Md. II* to *Md. V* result in small asymmetry parameters of η_Q ≈ 0.1, which are in good agreement with the experimentally observed ones (Table 4). The EFG for *Md. I*, considering two

isolated Al(4b) to a first approximation, does not significantly differ from that of only one isolated Al(4b) atom. Once more, this evidences the local character of the EFG that was recently also described for cationic substitution in $Sr_{1-x}Ba_xGa_2$.[33] For both calculations focusing on isolated Al(4b) sites the asymmetry parameter η_Q is almost zero. Thus, isolated Al(4b) sites are assigned to the observed NMR signal of Al(4b1). Models *Md. II* to *Md. V* cannot be distinguished by their formation energies or EFGs. However, *Md. II* shows the best agreement of the EFG values derived by experiment and QM calculations (**Error! Reference source not found.**).

Conclusions

The isotypic IPs $SrAl_4$—$SrGa_4$ and $BaAl_4$—$BaGa_4$ form two solid solutions that can be described as $M(Al_{1-x}Ga_x)_4$ with *M* = Sr and Ba, respectively, and crystallise in the $BaAl_4$ type in space group *I*4/*mmm*. Full miscibility is proven by XRD and DTA investigations in which powder XRD experiments show a minimum for the *a* lattice parameter at *x* = 0.5, which is due to local atomic order in the anionic sublattice.

Figure 6. Formation energies ΔE_f of $Sr(Al_{1-x}Ga_x)_4$ (top) as well as the difference $\Delta(\Delta E_f)$ for comparison with the binary phases $SrAl_4$ and $SrGa_4$ (bottom). Open circles correspond to the various SLS calculations; open triangles show data for varying local ordering schemes of Al(4b)/Al(5b) with *x* = 0.5. The data for $Ba(Al_{1-x}Ga_x)_4$ is shown in **Error! Reference source not found.**.

$M(Al_{1-x}Ga_x)_4$ with *M* = Sr, Ba and *x* = 0.975, 0.950, and 0.925 can be described as regimes of low Al substitution into a MGa_4 matrix with *M* = Sr, Ba and formulated as Al@MGa_4.

Solid-state ^{27}Al NMR investigations on magnetically aligned powder samples are very well suited to investigate different Al environments on a local atomic level. Especially the ST NMR signals are highly sensitive on the Al—Ga substitution degree and give an experimental proof for a preferred occupancy of the (4b) position by Al within the gallide matrix.

The trend of the lattice parameter is reproduced by QM calculations considering a preferred site occupation of Al(4b). In addition, the formation energies support this local order of the atoms. Various models of different local Al(4b)—Al(4b) pairs cannot be distinguished by their formation energies. Best agreement of respective calculated and measured EFG values is found for Al(4b) pairs in close distance too each other. Hence, the formation of Al(4b)—Al(4b) pairs next to isolated Al(4b) atoms is revealed by the combined application of NMR and QM investigations.

While already being well known to study ordered and disordered IPs influenced by cation substitution, this work enhances the XRD—NMR—QM approach to a next level since investigations of anionic disorder in IPs become accessible. Especially for the sought-after aluminides with high technological relevance this approach is likely to shed light into structure-bonding-property relationships and to be applied to an ever increasing range of technologically relevant metallic materials.

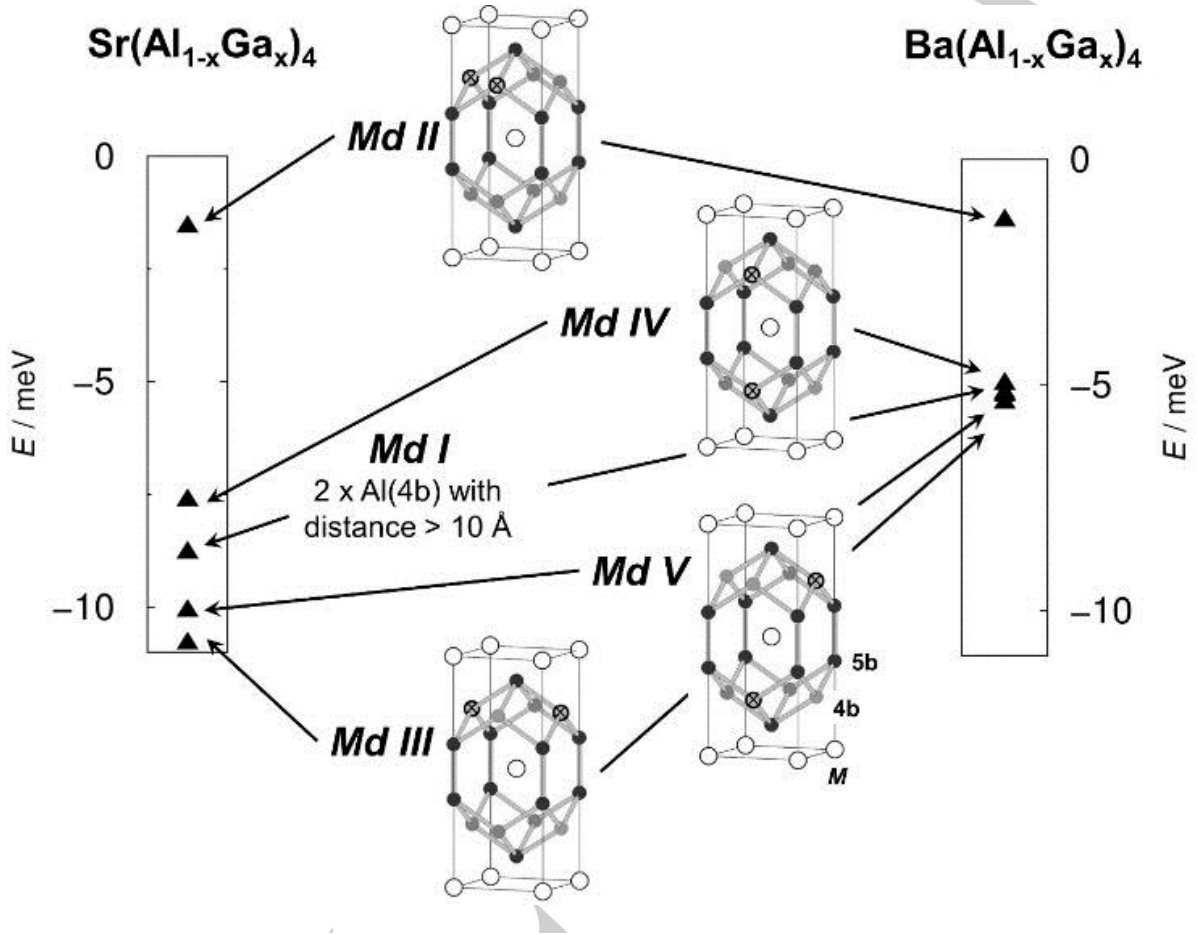

Figure 7. Relative energies (*E* / meV) for $Sr(Al_{1-x}Ga_x)_4$ (left) and $Ba(Al_{1-x}Ga_x)_4$ (right). Varying local Al—Al arrangements corresponding to model *Md. II* to *Md. V* are given with respect to a $BaAl_4$ type unit cell used in the centre of a 3×3×2 SLS calculation (middle). Details of the special Al arrangements are discussed in the text. Ga(4b) and Ga(5b) positions are visualised by grey and black circles, respectively. Al(4b) positions are marked by crosses. Open circles represent the cations *M* = Sr or Ba. The maximum of the energy differences is approx. 0.009 eV for $Sr(Al_{1-x}Ga_x)_4$ and 0.004 eV for $Ba(Al_{1-x}Ga_x)_4$, respectively.

Table 3. ^{27}Al NMR parameters of quadrupole coupling and signal shift interaction from NMR signal line shape analysis and QM calculations for $SrAl_4$ and $BaAl_4$. According to the site symmetry of the Al(4b) and Al(5b) atoms on Wyckoff position 4*d* ($\bar{4}m2$) and 4*e* (4*mm*) in space group *I*4/*mmm* an asymmetry parameter of $\eta = 0$ results.[17,30,50]

	$SrAl_4$				$BaAl_4$			
	Al(4b)		Al(5b)		Al(4b)		Al(5b)	
	NMR	QM	NMR	QM	NMR	QM	NMR	QM
V_{ZZ} / 10^{21} Vm^{-2}	1.74(2)	-1.85(2)	0.80(2)	-0.68(2)	2.06(2)	-2.23(2)	0.51(2)	-0.32
Δ_{iso} / ppm	1030(10)	-	564(10)	-	1128(10)	-	347(10)	-
Δ_{aniso} / ppm	0	-	100(10)	-	-54(10)	-	106(10)	-

Table 4. ^{27}Al NMR parameters of quadrupole coupling and signal shift interaction from NMR signal line shape analysis for $Sr(Al_{1-x}Ga_x)_4$ and $Ba(Al_{(1-x}Ga_x)_4$ with x = 0.975, 0.950, and 0.925. The respective ISC regimes and models for the local Al(4b) environments are given. Additionally, the QM calculated parameters considering model II are shown (see QM calculations andFigure 7 for further details).

$Sr(Al_{1-x}Ga_x)_4$ x =	0.975		0.950		0.925		QM	
ISC regime	2.5 % Al@$SrGa_4$		5.0 % Al@$SrGa_4$		7.5 % Al@$SrGa_4$			
Model	Al(4b1)	Al(4b2)	Al(4b1)	Al(4b2)	Al(4b1)	Al(4b2)	Al(4b1)	*Md. II*
V_{ZZ} / 10^{21} Vm^{-2}	1.99(2)	1.88(2)	2.00(2)	1.85(2)	1.99(2)	1.88(2)	-2.09	-1.924
η_Q	0	0.1(1)	0	0.1(1)	0	0.1(1)	0	0.11
Δ_{iso} / ppm	875(10)	931(10)	872(10)	916(10)	854(10)	937(10)	-	-
Δ_{aniso} / ppm	-57(10)	-67(10)	-65(10)	-72(10)	-72(10)	-31(10)	-	-
η_Δ	0	0	0	0	0	0	-	-
$Ba(Al_{1-x}Ga_x)_4$ x =	0.975		0.950		0.925		QM	
ISC regime	2.5 % Al@$BaGa_4$		5.0 % Al@$BaGa_4$		7.5 % Al@$BaGa_4$			
Model	Al(4b1)	Al(4b2)	Al(4b1)	Al(4b2)	Al(4b1)	Al(4b2)	Al(4b1)	*Md. II*
V_{ZZ} / 10^{21} Vm^{-2}	2.04(2)	1.93(2)	2.05(2)	1.97(2)	2.05(2)	1.97(2)	-2.14	-2.023
η_Q	0	0.1(1)	0	0.1(1)	0	0.1(1)	0	0.06
Δ_{iso} / ppm	1005(10)	1030(10)	1022(10)	1014(10)	1102(10)	999(10)	-	-
Δ_{aniso} / ppm	-35(10)	-73(10)	-39(10)	-45(10)	-339(10)	-70(10)	-	-
η_Δ	0	0	0	0	0	0	-	-

Experimental Section

Sample Preparation

Polycrystalline powder samples of $M(Al_{1-x}Ga_x)_4$ with *M* = Sr, Ba were prepared by three different solid-state synthesis methods depending on the Al amount of the respective sample (Table S1).[17] The starting materials Sr (Alfa Aesar, distilled dendritic pieces, 99.95 %), Ba (Alfa Aesar, crystalline dendritic pieces, 99.9 %), Al (ChemPur, pellets, 99.999 %), Al foil (0.1 and 0.25 mm thickness, 99.99 % and 99.997 %), and Ga (ChemPur, pellets < 8 mm, 99.999 %), precursors phases, and products were always handled under Ar atmosphere in a MBraun glove box system with $p(O_2;H_2O)$ < 0.1 ppm to avoid contamination and/or reaction with moisture of air.

Direct synthesis in Ta ampoules (method A): Appropriate mixtures of Sr, Ba, Al, and Ga for $Sr(Al_{1-x}Ga_x)_4$ ($0.6 \le x \le 1.0$) and $Ba(Al_{1-x}Ga_x)_4$ ($0.0 \le x \le 1.0$) were melt at approx. 950°C in a high-frequency furnace using sealed Ta ampoules. The Ta containers were enclosed in evacuated quartz glass ampoules, thermally treated at 800°C for 2 weeks and cooled down to ambient temperature with 10 K/min afterwards.

Synthesis via precursor AlGa alloy (method B): Side reactions of Al with the Ta ampoules impaired the synthesis of single phase materials for $Sr(Al_{1-x}Ga_x)_4$ with x = 0.5. Hence, a precursor AlGa alloy, showing a moderately lower melting point of approx. 400°C compared to Al metal with 660°C[17] was used. A 1:1 ratio of small Al and Ga pieces was homogenised at 420°C in an open Ta ampoule inside a tube furnace for 2 days. The resulting alloy (silver, metallic lustrous) was added to Sr in a respective ratio for $SrAl_2Ga_2$, sealed in a Ta ampoule, enclosed in evacuated quartz glass ampoules and slowly heated to 550°C within 6 hours. After a thermal treatment for 7 days at this temperature the sample was cooled down to ambient temperature with 10 K/min.

Synthesis via a pellet (method C): For $Sr(Al_{1-x}Ga_x)_4$ ($0.0 \le x < 0.5$) neither method A nor B succeed in single phase materials due to side reactions of Al with the container material. Therefore, we prepared thin Al ampoules out of Al foil and added the respective Sr and Ga amounts. The elements were pressed at 30 kN for 2 minutes and melted on the Cu coquille of an arc welder. The resulting pill was sealed in a Ta ampoule, thermally treated in a muffle furnace at 800°C for 2 weeks, and finally slowly cooled down to ambient temperature with 10 K/min.

Powder XRD and Lattice Parameter Determination

XRPD experiments were performed using a STOE & Cie (Darmstadt, Germany) STADI P diffractometer in transmission geometry with $CuK_{\alpha 1}$ radiation (λ = 1.54056 Å; Ge monochromator after Johann; measurements at Ω = 55°; image plate detector; internal standard LaB_6 with a = 4.15692 Å). The lattice parameters were determined using the same set of sample and internal standard reflections for the whole series of $M(Al_{1-x}Ga_x)_4$ with *M* = Sr, Ba (**Error! Reference source not found.**).[17] The WinCSD-2000 program package was used for the peak profile fitting and lattice parameter determinations.[51]

Single Crystal XRD

A single crystal of $Sr(Al_{1-x}Ga_x)_4$ with x = 0.925 was mounted on a glass fibre using crystal oil (Perfluoropolyalkylether AB128333 viscosity 1800 cSt., ABCR) and measured at 100(2) K under nitrogen gas flow. Intensity and geometry data were collected in ω-scan mode with an APEX CCD area detector on a Bruker D8 goniometer that was equipped with an Incoatec microsource with multilayer optics using $Mo_{K\alpha}$. For the low temperature measurement an Oxford Cryostream 700 cooler was utilised. Data processing and multi-scan absorption corrections were done using the programs SAINT+[52] and SADBS[53], respectively. Crystal structure solution and refinement were carried out with SHELXS-97 and SHELXL-2013, respectively.[54,55] Details of the data collection and handling are summarised in Table 1 and Table 2. Further details on the crystal structure investigations can be obtained from the Fachinformationszentrum Karlsruhe, 76344 Eggenstein-Leopoldshalfen, Germany (fax: (+49)7247808666, e-mail: crysdatat@fizkarlsruhe.de; http://www.fiz-karlsruhe.de/request_for_deposited_data.html) on quoting the depository number CSD-430628.

DTA Measurements

Samples of $M(Al_{1-x}Ga_x)_4$ with *M* = Sr, Ba were investigated by means of DTA using a Netzsch DSC 404C Pegasus under argon flow of 150 mL/min.[56,57] Approximately 50 mg of powdered sample were sealed in a niobium ampoule under argon atmosphere and measured between ambient temperature and 1200°C at heating/cooling rates of 5 $Kmin^{-1}$. An empty sealed niobium ampoule was used as reference material on a Netzsch DSC sample holder type S. Data analysis of the heating curves with respect to start, onset and maximum values of thermal effects was performed using the program Netzsch Proteus thermal analysis.[44,58]

Solid-State NMR Spectroscopy

NMR sample preparation and measurement techniques: Static ^{27}Al NMR experiments have been performed on both regular and magnetically aligned powder samples.[17,30–33] Therefore, the polycrystalline powder samples were mixed with two-component glue (UHU endfest 300) and filled into quartz glass tubes of 5 mm in diameter. The hardening process of the glue-powder suspension was done outside or inside the magnetic field to achieve regular and aligned powder samples, respectively. The NMR experiments were performed by using a Bruker AVANCE III spectrometer with a magnetic field of B_0 = 9.40 T. The corresponding ^{27}Al frequency is 104.269 MHz. All signals are referenced to a solution of $Al(NO_3)_3$ in D_2O.[59,60] The static (no sample spinning) NMR experiments were performed with a low-Q automatic tuning matching goniometer (ATMG) probe system[33]. Wideline measurements were performed on aligned powder samples using an echo sequence with pulses of equal duration (1.75 µs). To avoid lineshape distortions the interpulse delay was optimised to 100 – 200 µs. Regular powder samples were measured by applying a series of selective excitation experiments (frequency sweep)[17,30,61] with low power pulses of 50 and 25 µs duration for $SrAl_4$ and $BaAl_4$, respectively. All experiments were performed using eightfold cycle of pulse sequences with a cycle delay of 0.25 s.

Definitions and data analysis: The polycrystalline powder samples of $M(Al_{1-x}Ga_x)_4$ with *M* = Sr, Ba comprise a statistic distribution of the crystallite orientations in the pristine stage, which is described as regular powder.[17,30–33] As soon as these samples experience a strong magnetic field (such as the one of the NMR experiment) the crystallites align in a preferred orientation with respect to the direction of the magnetic field. This is due to the intrinsic anisotropic conductivity of the material and its interaction with the magnetic field, the so-called Lorentz force, which is minimised by the preferred orientation. Powder samples with crystallites in such a preferred orientation are referred to as aligned powders.[17,30–33] The dominant NMR interactions for $M(Al_{1-x}Ga_x)_4$ with *M* = Sr, Ba are quadrupolar coupling, chemical and Knight shift. The main component of the EFG V_{zz} and the asymmetry parameter η_Q describe the quadrupolar coupling.[30] The shift interactions, chemical shielding and Knight shift, cannot be separated experimentally and are therefore represented by the

following set of parameters: the complete isotropic Δ_{iso} and anisotropic shift Δ_{aniso} as well as the asymmetry parameter η_Δ.[30,33] NMR signal lineshape analysis was performed using MATLAB scripts that enabled simultaneous least square fits of multiple NMR data sets for one sample. For aligned powders a reduced powder average was implemented to describe the orientation of B_0 with respect to the NMR coupling tensors based on QM calculations and the crystallite orientations.[46] For all local atomic environments with $\eta_\Delta = \eta_Q = 0$ the interaction tensors main component is parallel to the crystallographic *c* axis. With asymmetry parameters deviating from zero the coupling tensor can take other orientation. For aligned crystallites the *c* axis is perpendicular to B_0. Therefore for $\eta_\Delta = \eta_Q = 0$ the tensor main components are disc-like distributed with respect to B_0. A more complex orientation of the NMR coupling tensors is possible in case of $\eta_\Delta / \eta_Q \neq 0$ since the symmetry constraints no longer exist.[17,33] As already successfully established for similar fits of Ga NMR data, we carefully checked the influence of non-equal orientations of the shift and quadrupole tensor on the NMR signal fit and found no significant difference on the fit quality for the present Al NMR data. Hence, we assume identical orientations of shift and quadrupole interaction tensors throughout the data analysis.

QM Calculations

The VASP program package[45] based on the Plane Augmented Waves (PAW)[62] method using the Local Density Approximation (LDA) was employed for crystal structure optimisations. For all calculations the energy cut-off for the plane waves was set to 500 eV, the convergence criteria for the electronic relaxation was set to 1×10^{-6} eV and for the ionic relaxation to -5×10^{-3} eV. Nine models using the $BaAl_4$ type unit cell for $M(Al_{1-x}Ga_x)_4$ with *M* = Sr, Ba and *x* = 0, 0.125, 0.25, 0.375, 0.5, 0.625, 0.75, 0.875, 1 were utilised with a 10×10×5 k-grid. An estimation of the formation energies of the elements Sr(fcc)[63], Ba(bcc)[63], Al(fcc)[39,63], and α-Ga[40,63] was performed applying the identical convergence criteria and a 30×30×30 k-grid. The 3×3×2 SLS of $M(Al_{1-x}Ga_x)_4$ with *M* = Sr, Ba and *x* = 0.007, 0.014, 0.986, and 0.993 with up to 180 atoms, were used to model isolated and adjacent substitution centres. The SLS were generated according to the Bärnighausen formalism.[47] To check for the influence on the symmetry constraints the calculations were also performed in space group *P*1. These were sampled with a 4×4×2 k-grid applying the same convergence criteria mentioned above. After structure optimisation in the VASP program package the EFG was calculated using the Full Potential Linear Augmented Plane Wave (FP-LAPW) method as implemented in the Wien2k code.[46] As exchange and correlation functional the build in GGA PBE option was selected.[62] As basis set size we chose $R_{MT}\times K_{max} = 7$ and the default separation energy of -6.0 Rydberg for all calculations. The unit cells of the binary compounds were sampled with an 8×8×8 k-grid and the SLS with a 2×2×1 k-grid, respectively.

Acknowledgements

We gratefully acknowledge Prof. Ulli Engert (Aachen, Germany) for fruitful discussions on the single crystal XRD experiments and thank Dr. Paul Müller (Aachen, Germany) for powder XRD measurements. We thank Raphaela Kannengießer, Patrick Offer, and Christian Schwab (all RWTH Aachen University, Aachen, Germany) for their help during synthesis and NMR measurements. Dr. Marcus Schmidt and Susann Scharsach (MPI CPfS, Dresden, Germany) are thanked for DTA measurements. This work was partially supported by the Excellence Initiative (O.P., B.M., V.P., and F.H.).

Keywords: chemical bonding • intermetallic phases • NMR spectroscopy • quantum mechanical calculations • substitutional disorder

[1] A. Simon, *Angew. Chem.* **1983**, *95*, 94–113.

[2] Z.-A. Ren, Z.-X. Zhao, *Adv. Mater.* **2009**, *21*, 4584–4592.

[3] R. Pöttgen, D. Johrendt, *Z. Naturforsch.* **2008**, *63b*, 1135–1148.

[4] C. Felser, G. Fecher, B. Balke, *Angew. Chem. Int. Ed.* **2007**, *46*, 668–699.

[5] C. Felser, G. Fecher, B. Balke, *Angew. Chem.* **2007**, *119*, 680–713.

[6] J. Scootsman, D. Chung, M. Kanatzidis, *Angew. Chem. Int. Ed.* **2009**, *48*, 8616–8639.

[7] J. Scootsman, D. Chung, M. Kanatzidis, *Angew. Chem.* **2009**, *121*, 8768–8792.

[8] G. S. Nolas, *Thermoelectrics: Basic Principles and New Materials Developments*, Springer, Berlin, **2001**.

[9] M. Armbrüster, K. Kovnir, M. Friedrich, D. Teschner, G. Wowsnick, M. Hahne, P. Gille, L. Szentmiklósi, M. Feuerbacher, M. Heggen, et al., *Nat. Mater.* **2012**, *11*, 690–693.

[10] G. Sauthoff, *Intermetallics*, Wiley-VCH, Weinheim, **1995**.

[11] J. H. Westbrook, R. L. Fleischer, *Intermetallic Compounds, Volume 4: Magnetic, Electrical and Optical Properties and Applications of Intermetallic Compounds*, Wiley, Chichester, **2000**.

[12] J.-M. Dubois, E. Belin-Ferré, M. Feuerbacher, *Introduction to the Science of Complex Metallic Alloys*, Wiley-VCH, Weinheim, **2010**.

[13] R. Nesper, *Angew. Chem. Int. Ed.* **1991**, *30*, 789–817.

[14] R. Nesper, *Angew. Chem.* **1991**, *103*, 805–834.

[15] Y. Grin, U. Schwarz, W. Steurer, Wiley-VCH Verlag GmbH & Co. KGaA, Weinheim, **2007**, pp. 62–68.

[16] Y. Grin, *Wiss. Z. Techn. Univers. Dresden* **2000**, *49*, 16–20.

[17] O. Pecher, NMR Spectroscopy on Intermetallic Phases in the Systems AE–Al–Ga with AE = Ca, Sr, and Ba Experimental and Theoretical Investigations of Chemical Bonding, RWTH Aachen University, **2013**.

[18] O. Pecher, F. Haarmann, *Nachr. Chem.* **2013**, *61*, 1018–1021.

[19] R. Ang, Z. C. Wang, C. L. Chen, J. Tang, N. Liu, Y. Liu, W. J. Lu, Y. P. Sun, T. Mori, Y. Ikuhara, *Nat. Commun.* **2015**, *6*, 6091.

[20] O. Ambacher, *J. Phys. D Appl. Phys.* **1998**, *31*, 2653–2710.

[21] I. M. Watson, *Coord. Chem. Rev.* **2013**, *257*, 2120–2141.

[22] A. J. Baca, J.-H. Ahn, Y. Sun, M. Meitl, E. Menard, H.-S. Kim, W. M. Choi, D.-H. Kim, Y. Huang, J. A. Rogers, *Angew. Chem. Int. Ed.* **2008**, *47*, 5524–5542.

[23] J.-H. Kang, T. Ingendahl, J. van Appen, R. Dronskowski, W. Bleck, *Mater. Sci. Eng. A* **2014**, *614*, 122–128.

[24] P. K. Allan, J. M. Griffin, A. Darwiche, O. J. Borkiewicz, K. M. Wiaderek, K. W. Chapman, A. J. Morris, P. J. Chupas, L. Monconduit, C. P. Grey, *J. Am. Chem. Soc.* **2016**, *138*, 2352–2365.

[25] R. Pöttgen, D. Johrendt, *Intermetallics: Synthesis, Structure, Function*, De Gruyter, **2014**.

[26] D. Kußmann, R. Pöttgen, U. C. Rodewald, C. Rosenhahn, B. D. Mosel, G. Kotzyba, B. Künnen, *Z. Naturforsch.* **1999**, *54b*, 1155–1164.

[27] Z. Ban, M. Sikirica, *Acta Cryst.* **1965**, *18*, 594–599.

[28] F. Merlo, M. Pani, M. L. Fornasini, *J. Less-Common Met.* **1990**, *166*, 319–327.

[29] B. Eisenmann, H. Schäfer, *Z. anorg. allg. Chem.* **1974**, *403*, 163–172.

[30] F. Haarmann, *Quadrupolar NMR of Intermetallic Compounds*, John Wiley & Sons, Ltd, Chichester, **2011**.

[31] F. Haarmann, K. Koch, D. Grüner, W. Schnelle, O. Pecher, R. Cardoso-Gil, H. Borrmann, H. Rosner, Y. Grin, *Chem. Eur. J.* **2009**, *15*, 1673–84.

[32] F. Haarmann, K. Koch, P. Jeglič, O. Pecher, H. Rosner, Y. Grin, *Chem. Eur. J.* **2011**, *17*, 7560–8.

[33] O. Pecher, B. Mausolf, K. Lamberts, D. Oligschläger, C. Niewieszol (née Merkens), U. Englert, F. Haarmann, *Chem. Eur. J.* **2015**, *21*, 13971–13982.

[34] F. Haarmann, Y. Prots, *Z. anorg. allg. Chem* **2006**, *632*, 2135.

[35] O. Pecher, F. Haarmann, *Z. anorg. allg. Chem.* **2008**, *634*, 2069.

[36] O. Pecher, F. Haarmann, *Z. anorg. allg. Chem.* **2012**, *638*, 1622.

[37] W. F. Harms, M. Wendorff, C. Röhr, *Z. Naturforsch., B Chem. Sci.* **2006**, *62*, 177–194.

[38] F. Haarmann, M. Armbrüster, Y. Grin, *Chem. Mater.* **2007**, *19*, 1147–1153.

[39] A. Palenzona, *J. Less-Common Met.* **1972**, *29*, 289–292.

[40] B. D. Sharma, J. Donohue, *Z. Krist.* **1962**, *117*, 293–300.

[41] G. J. Miller, F. Li, H. F. Franzen, *J. Am. Chem. Soc.* **1993**, *115*, 3739–3745.

[42] C. B. Alcock, V. P. Itkin, *Bull. Alloy Phase Diagrams* **1989**, *10*, 624–630.

[43] V. P. Itkin, C. B. Alcock, *J. Phase Equilib.* **1993**, *14*, 518–524.

[44] W. J. Boettinger, U. R. Kattner, J. H. Perepezko, *DTA and Heat-Flux DSC Measurements of Alloy Melting and Freezing*, National Institute Of Standards And Technology, Washington, DC, **2006**.

[45] G. Kresse, J. Furthmüller, *Phys. Rev. B* **1996**, *54*, 11169–11186.

[46] P. Blaha, K. Schwarz, G. K. H. Madsen, D. Kvasnicka, J. Luitz, *WIEN2k, An Augmented Plane Wave Plus Local Orbitals Program for Calculating Crystal Proporties*, Vienna University Of Technology, Austria, Vienna, **2001**.

[47] H. Bärnighausen, *Commun. Math. Chem.* **1980**, *9*, 139–175.

[48] R. Dronskowski, *Computational Chemistry of Solid State Materials*, WILEY-VCH Verlag, **2005**.

[49] Y. Wang, C. Woodward, S. H. Zhou, Z.-K. Liu, L.-Q. Chen, *Scr. Mater.* **2005**, *52*, 17–20.

[50] K. R. Jeffrey, G. Penner, in *NMR Crystallogr.*, John Wiley & Sons, Chichester, West Sussex, **2009**, pp. 387–412.

[51] L. Akselrud, Y. Grin, *J. Appl. Crystallogr.* **2014**, *47*, 803–805.

[52] *SAINT+ (Version 6.02) - Program for Reduction of Data Collected on Bruker CCD Area Detector Diffractometer*, Bruker AXS Inc., Madison, WI, USA, **1999**.

[53] G. M. Sheldrick, *SADABS (Version 2.03). Program for Empirical Absorption Correction of Area Detector Data*, University Of Goettingen, Germany, **1996**.

[54] G. M. Sheldrick, *Acta Cryst. A* **2008**, *64*, 112–122.

[55] G. M. Sheldrick, *Acta Crystallogr. C* **2015**, *71*, 3–8.

[56] *Normausschuß Materialprüfung (NMP) Im DIN Deutsches Institut Für Normung E. V., Deutsche Norm DIN 51007, Thermische Analyse (TA), Differenzthermoanalyse (DTA), Grundlagen*, Beuth Verlag GmbH, Berlin, **1994**.

[57] *Normausschuß Materialprüfung (NMP) Im DIN Deutsches Institut Für Normung E. V., Deutsche Norm DIN 51005, Thermische Analyse (TA), Begriffe*, Beuth Verlag GmbH, Berlin, **2005**.

[58] Netsch-Gerätebau, *Netzsch Proteus Thermal Analysis (Version 4.8.3)*, Selb, Bayern, Germany, **2006**.

[59] R. K. Harris, E. D. Becker, S. M. Cabral de Menezes, R. Goodfellow, P. Granger, *Magn. Reson. Chem.* **2002**, *40*, 489–505.

[60] R. K. Harris, E. D. Becker, *J. Magn. Reson.* **2002**, *156*, 323–326.

[61] O. Pecher, P. M. Bayley, H. Liu, Z. Liu, N. M. Trease, C. P. Grey, *J. Magn. Reson.* **2016**, *265*, 200–209.

[62] H. M. Petrilli, P. E. Blöchl, P. Blaha, K. Schwarz, *Phys. Rev. B* **1998**, *57*, 14690–14697.

[63] F. Haarmann, B. Mausolf, *Lattice and Positional Parameter Obtained by Structure Optimization Sr(fcc) a = 5.7880 Å, Ba(bcc) a = 4.7695 Å, Al(fcc) a = 3.9843 Å, and Alpha-Ga a = 4.4345 Å, B = 7.5296 Å, c = 4.4528 Å, Ga X = 0, Y = 0.1556, Z = 0.0831.*, RWTH Aachen University (Germany), **2016**.

Entry for the Table of Contents (Please choose one layout)

Layout 1:

FULL PAPER

Text for Table of Contents

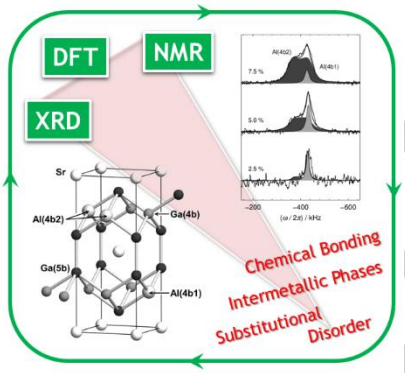

*Oliver Pecher, Bernhard Mausolf, Volker Peters, Kevin Lamberts, Alexander Korthaus, and Frank Haarmann**

Page No. – Page No.

Unravelling local atomic order of the anionic sublattice in $M(Al_{1-x}Ga_x)_4$ with M = Sr and Ba by NMR spectroscopy and quantum mechanical modelling